2014

Dynamics of Coupled Noisy Neural Oscillators with Heterogeneous Phase Resetting Curves

Cheng Ly
Virginia Commonwealth University, cly@vcu.edu

DYNAMICS OF COUPLED NOISY NEURAL OSCILLATORS WITH HETEROGENEOUS PHASE RESETTING CURVES *

CHENG LY†

Abstract. Pulse-coupled phase oscillators have been utilized in a variety of contexts. Motivated by neuroscience, we study a network of pulse-coupled phase oscillators receiving independent and correlated noise. An additional physiological attribute, heterogeneity, is incorporated in the phase resetting curve (PRC), which is a vital entity for modeling the biophysical dynamics of oscillators. An accurate probability density or mean field description is large dimensional, requiring reduction methods for tractability. We present a reduction method to capture the pairwise synchrony via the probability density of the phase differences, and explore the robustness of the method. We find the reduced methods can capture some of the synchronous dynamics in these networks. The variance of the noisy period (or spike times) in this network is also considered. In particular, we find phase oscillators with predominately positive PRCs (type 1) have larger variance with inhibitory pulse-coupling than PRCs with a larger negative regions (type 2), but with excitatory pulse-coupling the opposite happens – type 1 oscillators have lower variability than type 2. Analysis of this phenomena is provided via an asymptotic approximation with weak noise and weak coupling, where we demonstrate how the individual PRC alters variability with pulse-coupling. We make comparisons of the phase oscillators to full oscillator networks and discuss the utility and shortcomings.

Key words. Neural oscillators, phase resetting curve (PRC), heterogeneity, Fokker-Planck equation, weak pulse-coupling, weak noise

AMS subject classifications. 37N25, 92C20

1. Introduction.

Heterogeneity is a realistic feature that is often neglected in stochastic networks because the dynamics of such homogeneous systems are already complicated. Tractable analysis of stochastic systems often involve exploiting homogeneity and focusing on average quantities that can be captured by various methods. However, an undeniable feature of biological systems is the large amount of heterogeneity in the intrinsic dynamics [37]. In recent years, intrinsic heterogeneity in model neural networks has gained increasing attention but such models are still understudied.

Two important signatures of neural activity are the level of synchrony and variability. Synchrony (i.e., correlation) and variability have implications on neural coding, as well pathologies, thus acquiring a mechanistic understanding of their dynamics is crucial. Various studies have shown that synchrony/correlation can arise from direct coupling [57, 28, 39, 24], external forcing [27, 13], common noisy input [53, 47, 18, 42, 38, 7], among other features. The dynamics of how these entities modulate is confounded by neural network attributes [45, 44, 33, 51]. Spiking activity is known to be variable or noisy, and understanding how this feature is altered, even in specific regimes, is a central focus in computational neuroscience. The models considered here are oscillators, where each cell is assumed to receive enough drive to fire action potentials repetitively. Despite these assumptions, these class of models have been successfully applied in neuroscience [48] and beyond [58, 4, 30].

Neural oscillators have an associated phase-resetting curve (PRC). The PRC is an experimentally measurable quantity that specifies how perturbations change the time until the next spike for neural oscillators. Since the PRC is known to depend

*Received:

†CLy@vcu.edu; Department of Statistical Sciences and Operations Research, Virginia Commonwealth University, Richmond, VA 23284-3083

on biophysical parameters, ionic currents, firing rate, etc. [17, 48], one would expect PRCs to be heterogeneous. There has been recent experimental work that shows the large degree of intrinsic heterogeneity of mitral cells in the olfactory bulb [9]. They found that the PRCs of these cells varied greatly. Zhou et al. [61] recently considered two heterogeneous uncoupled oscillators with different PRCs and intrinsic frequencies subject to independent and common noise. The noise they considered had temporal correlations (i.e., Ornstein-Uhlenbeck processes). These authors found that in the low input correlation limit, that heterogeneity can lead to more synchronous behavior – the synchrony comes from the common noise drive. Along with correlated noisy background inputs and heterogeneity, coupling can have a significant effect on synchrony *and* variability. To this end, we study a network of heterogeneous noisy neural oscillators that are pulse-coupled, where each neuron is subject to noisy background inputs with independent and common parts. We incorporate intrinsic heterogeneity by allowing all of the PRCs to vary, but assume the intrinsic frequencies are all the same because the network is already large dimensional. A dimension reduction method is proposed and tested on a large phase oscillator network. We find the theory can qualitatively capture the pairwise synchronous dynamics of this network, compared to computationally intensive Monte Carlo simulations. The results are compared to a heterogeneous coupled Morris-Lecar network, and the same trend is qualitatively observed.

We also study how coupling alters the variability of this neural oscillator network and find that this crucially depends on PRC type. In particular, if the PRCs are normalized to have L_2-norm of 1, then with inhibitory pulse-coupling we find that neurons with large positive regions in their PRC (i.e., type I) have larger variance in their spike times (or periods) than neurons with larger negative regions (i.e., type II); with excitatory pulse-coupling, the opposite happens where neurons with type II PRCs have larger variability than type I neurons. An asymptotic formula is presented to clearly explain these observations. The results are tested on full oscillator systems, and we find surprisingly that the same phenomena are not observed. Further examination of the theory for the reduced phase oscillators elucidates why the results are not robust; the asymptotic analysis demonstrates that the conditions of the PRC are stringent to observe the phenomena with type II PRCs. In total, this work provides further insights into the study of coupled heterogeneous noisy oscillators.

2. Heterogeneous noisy neural oscillators. Consider a population of N distinct coupled neural oscillators receiving independent and correlated white noise. Let $X_j \in \mathbb{R}^n$ denote the variables of the $j^{th} \in \{1, 2, \ldots, N\}$ oscillator type. The equation describing the evolution of X_j is:

$$\frac{dX_j}{dt} = F(X_j) + \tilde{\alpha}\frac{1}{N-1}\sum_l G(X_j, X_l) + \tilde{\sigma}\vec{\xi}_j(t) =: F(X_j) + \epsilon_j \tag{2.1}$$

where $\tilde{\sigma} \ll 1$ is the power of the noise, $\tilde{\alpha} \ll 1$ is the coupling strength, and $\vec{\xi}_j(t)$ are stationary correlated white noise processes with zero mean and unit variance. We assume that the noise and coupling only affects the voltage (first) component, which holds for a wide class of neuron models (i.e., ϵ_j has 0 in all components except the first). To obtain a tractable phase model where a phase reduction can be applied, we assume that the uncoupled and unperturbed system $\frac{dX_j}{dt} = F(X_j)$ (i.e., setting $\tilde{\sigma} = \tilde{\alpha} = 0$) has an asymptotically stable limit cycle, $X_0(t) = X_0(t + T)$. We further assume that the coupling is uniform (all-to-all), and that the intrinsic frequencies

without perturbations are all the same. Although there are several assumptions made about the underlying network, the probability density description below (equation (2.4)) is still complicated and high dimensional.

A phase reduction is applied to the model above (equation 2.1) to obtain a network of phase oscillator models [28]. The phase reduction we evoke here is standard and has been described previously by many authors [42, 2, 6] (for further details, see [33, 34, 36] in particular). Note that there are other phase reductions with that can be utilized (see [60]); we focus on the case where the oscillators return to the limit cycle fast with weak perturbations as described in Teramae et al. [54]. Recent work has addressed the case of strong perturbations [56, 10, 29] requiring more variables than just the phase, which can lead to different dynamics [43].

The result of applying the phase reduction are the following system of Itô stochastic differential equations:

$$\frac{d\Theta_j}{dt} = 1 + \alpha\Delta_j(\Theta_j)\frac{1}{N-1}\sum_{k\neq j} P(\Theta_k) + \frac{\sigma^2}{2}\Delta_j(\Theta_j)\Delta_j'(\Theta_j) + \sigma\Delta_j(\Theta_j)\xi_j(t) \tag{2.2}$$

where the noise has zero mean $\langle\xi_j(t)\rangle = 0$ and can be correlated: $\langle\xi_j(t)\xi_k(t)\rangle = c\delta(t-t')$ when $j \neq k$, $c \in [0,1)$, and $\langle\xi_j(t)\xi_j(t')\rangle = \delta(t-t')$. Without loss of generality, the phase variables Θ_j take on values in [0,1). The dynamics of the oscillator depend crucially on Δ_j, the *Phase Resetting Curve* or PRC of the neuron. The PRC Δ_j vanishes at the end points 0 and 1 because in neurons, perturbations have no (or negligible) effect on the dynamics at the moment of a spike. Finally, the function $P(\Theta)$ represents the pulse-coupling, which has larger values when Θ is near 0 or 1 (spiking) to mimic the effect of presynaptic neurons.

Stochastic systems are often characterized by a probability density equation, or Fokker-Planck [50, 19]. Let

$$\Pr\left(\vec{\Theta}(t) \in (\vec{\theta}, \vec{\theta} + d\vec{\theta})\right) = \varrho(\vec{\theta}, t)\, d\vec{\theta}. \tag{2.3}$$

where the phase variables $\vec{\Theta} \in [0,1)^N$ represent the N distinct oscillators. The corresponding Fokker-Planck equation of the entire network is:

$$\begin{aligned}\frac{\partial\varrho}{\partial t} = &-\sum_{j=1}^{N}\frac{\partial}{\partial\theta_j}\left\{\left[1 + \alpha\frac{\Delta_j(\theta_j)}{N-1}\sum_{k\neq j}P(\theta_k) + \frac{\sigma^2}{2}\Delta_j(\theta_j)\Delta_j'(\theta_j)\right]\varrho - \frac{\sigma^2}{2}\frac{\partial}{\partial\theta_j}\Big\{\Delta_j^2(\theta_j)\varrho\Big\}\right\} \\ &+c\sigma^2\sum_{j<k}\frac{\partial^2}{\partial\theta_j\partial\theta_k}\Big\{\Delta_j(\theta_j)\Delta_k(\theta_k)\varrho\Big\}\end{aligned} \tag{2.4}$$

with periodic boundary condition in all coordinates θ_j: $\varrho(\ldots,\theta_j = 0,\ldots) = \varrho(\ldots,\theta_j = 1,\ldots)$ and normalization $\int_0^1 \varrho(\vec{\theta}, t)\, d\vec{\theta} = 1$.

3. Pairwise synchrony of noisy heterogeneous neural oscillators. An important signature of neural networks is the level of synchrony of their activity. Quantifying synchrony of the entire network is difficult because the probability density of all N phases (equation (2.4)) is generally large dimensional (when $N \geq 3$). We thus focus on pairwise synchrony of the network because 2-dimensional probability density equations can be solved numerically. The statistics of all $\frac{N(N-1)}{2}$ distinct

pairs of neurons collectively provides a reasonable measure of synchrony of the entire network.

Let us integrate out all of the variables in equation (2.4) in the steady-state, except the distinguished two variables of interest (θ_1 and θ_2 without loss of generality). The result is:

$$\begin{aligned}0 = &-\sum_{j=1}^{2}\frac{\partial}{\partial\theta_j}\left\{\left[1+\frac{\sigma^2}{2}\Delta_j(\theta_j)\Delta_j'(\theta_j)\right]\rho - \frac{\sigma^2}{2}\frac{\partial}{\partial\theta_j}\Big\{\Delta_j^2(\theta_j)\rho\Big\} + \alpha\frac{\Delta_j(\theta_j)}{N-1}\sum_{k\neq j}\int P(\theta_k)\varrho\, d\tilde{\theta}\right\}\\ &+c\frac{\sigma^2}{2}\frac{\partial^2}{\partial\theta_1\partial\theta_2}\Big\{\Delta_1(\theta_1)\Delta_2(\theta_2)\rho\Big\} + c\frac{\sigma^2}{2}\sum_{l,k\neq 1,2}\int\frac{\partial^2}{\partial\theta_l\partial\theta_k}\Big\{\Delta_l(\theta_l)\Delta_k(\theta_k)\varrho\Big\}\, d\tilde{\theta}\end{aligned} \tag{3.1}$$

where

$$\rho(\theta_1,\theta_2) = \int\varrho(\vec{\theta})\, d\tilde{\theta} := \int\varrho(\vec{\theta})\, d\theta_3\ldots d\theta_N. \tag{3.2}$$

This equation is not closed because there are still terms with the full density ϱ. Fortuitously, all of the cross diffusion terms with the other $N-2$ phase variables (2nd term on the 2nd line of equation (3.1)) vanish because integrating both θ_l and θ_k results in evaluating $\Delta_l\Delta_k\varrho$ at the endpoints $\theta_{l,k}=0,1$, where the PRC Δ vanishes. Therefore, we focus on

$$\frac{1}{N-1}\sum_{k\neq j}\int P(\theta_k)\varrho\, d\tilde{\theta}$$

to close the system. A term in this sum amounts to integrating $P(\theta_k)$ against the marginal density of $(\theta_1,\theta_2,\theta_k)$, except when $k=1,2$ where there is no issue of closure. The following approximation is made:

$$\rho(\theta_1,\theta_2,\theta_k) = \rho(\theta_1,\theta_2)\rho(\theta_k|\theta_1,\theta_2) \approx \rho(\theta_1,\theta_2)f(\theta_k) \tag{3.3}$$

where the conditional density of θ_k given (θ_1,θ_2) is approximated by the marginal density of θ_k: $f(\theta_k)$. This approximation is questionable when the coupling strength is large or when the background correlation level c is relatively large because Θ_k will be highly dependent on (Θ_1,Θ_2). Various measurements of background correlation in neural networks suggest that although c varies, it is generally not 'large' [12].

With this approximation, the resulting equation is:

$$\begin{aligned}0 = &-\sum_{j=1}^{2}\frac{\partial}{\partial\theta_j}\left\{\left[1+\frac{\sigma^2}{2}\Delta_j(\theta_j)\Delta_j'(\theta_j)+\alpha\Delta_j(\theta_j)\left\langle\left\langle P(\theta_j)\right\rangle\right\rangle\right]\rho - \frac{\sigma^2}{2}\frac{\partial}{\partial\theta_j}\Big\{\Delta_j^2(\theta_j)\rho\Big\}\right\}\\ &+c\frac{\sigma^2}{2}\frac{\partial^2}{\partial\theta_1\partial\theta_2}\Big\{\Delta_1(\theta_1)\Delta_2(\theta_2)\rho\Big\}\end{aligned} \tag{3.4}$$

where the two angular brackets around P denote averaging over the distribution of Θ_k *and* arithmetically averaging over all k phase variables:

$$\left\langle\left\langle P(\theta_j)\right\rangle\right\rangle := \frac{1}{N-1}\sum_{k\neq j}\int P(\theta_k)\, d\Theta_k. \tag{3.5}$$

The marginal density $f(\theta_k)$ still needs to be calculated in order to use equation (3.4). Integrating out all $N-1$ variables and making a similar approximation results in the following equation for $f(\theta_k)$:

$$\begin{aligned} \frac{\sigma^2}{2}\frac{d^2}{d\theta^2}\Big\{\Delta_k^2(\theta)f(\theta)\Big\} &= \frac{d}{d\theta}\left\{\left[1+\frac{\sigma^2}{2}\Delta_k(\theta)\Delta_k'(\theta)+\alpha\Delta_k(\theta)\left\langle\langle P\rangle\right\rangle\right]f(\theta)\right\} \\ f(0) &= f(1) \\ \int_0^1 f(\theta)\,d\theta &= 1. \end{aligned} \tag{3.6}$$

To close the system, we assume $\alpha = 0$ in equation (3.6) (otherwise the PDEs are nonlinear and may not be solvable) and utilize the weak noise and weak coupling assumption to derive an analytic formula for $f(\theta_k)$. Briefly, this involves expanding $f(\theta) = f_0(\theta) + \varepsilon f_1(\theta) + O(\varepsilon^2)$, collecting terms of the same order and imposing solvability conditions via the Fredholm Alternative to get:

$$f(\theta) \approx 1 + \frac{\sigma^2}{2}\Delta_k\Delta_k'. \tag{3.7}$$

A similar derivation is described in greater detail in [34] for a related noisy oscillator equation (also see [36]). Since there are a large number (N) of different marginal densities to be calculated, the analytic solution (3.7) is advantageous over a numerical 1-d PDE solution because it is faster to compute.

We now have a closed system of equations that approximates the probability density function of any desired pair of oscillators. The crucial quantity that measures the synchrony of a pair of neural oscillators is the density of the phase difference:

$$p(\phi = \theta_k - \theta_j) = \int_0^1 \rho(\theta_j, \phi+\theta_j)\,d\theta_j, \quad \phi \in (-1/2, 1/2). \tag{3.8}$$

Assuming the system is well-behaved and ergodic, $p(\phi)$ is a measure of the proportion of time that the pair of neurons have a particular phase difference. If $p(\phi)$ is sharply peaked at 0, then the neurons are synchronous; if there is a sharp peak at $\phi \neq 0$, then the pair are phase-lagged by that amount, etc.

3.1. Comparison of simulations with reduction method. The reduction for $\rho(\theta_j, \theta_k)$ is implemented and compared on a network of $N = 1000$ phase oscillators, where the PRCs are of the form (see Figure 3.1A):

$$\Delta_j(\theta) = k_j\Big[-\sin(2\pi\theta+\gamma_j)+\sin(\gamma_j)\Big], \quad \gamma_j \in [0, \pi/2]. \tag{3.9}$$

Although PRCs can be vastly different than these, the canonical type I ($\gamma_j = \pi/2, \Delta = 1+\cos(2\pi\theta)$) and type II ($\gamma_j = 0, \Delta = -\sin(2\pi\theta)$) PRCs are of this form [49, 21, 15]. This dichotomy has deep implications for the onset of repetitive firing with increased current injection [15]. The values γ_j are chosen from a specified distribution, which we set to be a uniform distribution. The normalizing constant $k_j = \frac{1}{\sqrt{\sin^2(\gamma_j)+1}}$ ensures the L_2-norm of all Δ_j are equal to 1. The L_2-norm of Δ appears in an asymptotic formula for the density of the phase difference of two identical uncoupled neural oscillators receiving correlated noise [38], and is also the lowest order approximation term of the variance of the random spike times (or interspike interval). Thus, this is

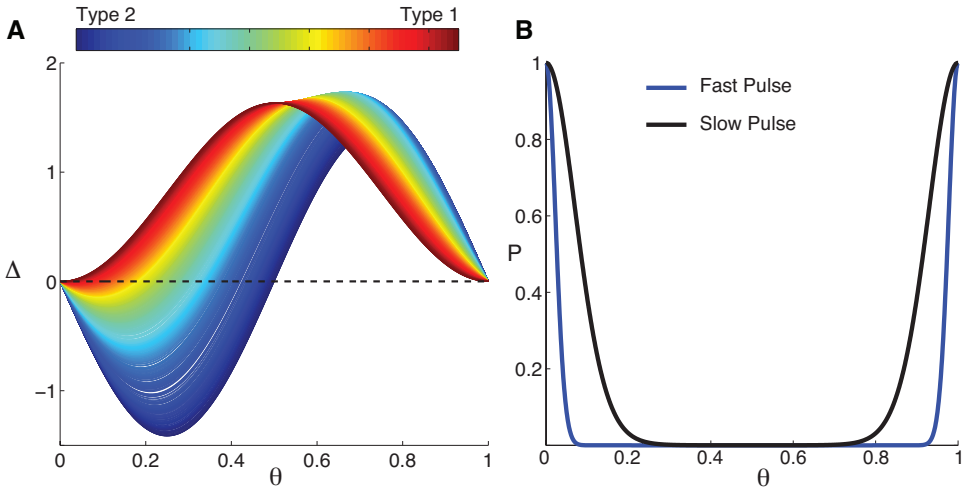

FIG. 3.1. *PRCs and Pulse of phase oscillator network*

A network of $N = 1000$ phase oscillators is considered, where the PRC $\Delta_j(\theta) = k_j[-\sin(2\pi\theta+\gamma_j)+\sin(\gamma_j)]$, for $\gamma_j \in [0, \frac{\pi}{2}]$. The normalization factor $k_j = \frac{1}{\sqrt{\sin^2(\gamma_j)+1}}$ insures that they all have the same L_2-norm: $\int_0^1 \Delta_j^2(\theta)\, d\theta = 1$. The parameter a_j is randomly chosen from a uniform distribution. (A) The distinct PRCs: red is canonical type I ($\gamma = \frac{\pi}{2}$) and blue is purely sinusoidal type II ($\gamma = 0$). (B) The pulse coupling function $P(\theta) = e^{-\beta(1-\cos(2\pi\theta))}$ can either be fast ($\beta = 50$) or slower decaying ($\beta = 5$).

a reasonable way to normalize and fairly compare heterogeneous PRCs. The pulse coupling is of the form:

$$P(\theta) = e^{-\beta(1-\cos(2\pi\theta))} \tag{3.10}$$

to model synaptic communication the occurs only around spiking (see Figure 3.1B).

With relatively fast pulses ($\beta = 50$), modest correlation $c = 0.25$, and inhibitory pulse-coupling $\alpha = -2$, the reduction method captures the wide variety of density of phase differences $p(\phi)$ in the same coupled network (same parameters) of particular pairs where the behavior ranges from synchronous (Figure 3.2B), partially phase-locked (Figure 3.2D), or asynchronous (Figure 3.2A). The Monte Carlo simulations (500,000 points in each histogram) are the red-dashed lines that measure the average time that pairs have a particular phase difference, and the black curves are solutions to closed two dimensional Fokker-Planck equations. The theory holds for excitatory pulse-coupling $\alpha = 2$ (Figure 3.2E–H), although by eye one could argue the match is not as good. However, note that even the skew and multiple humps in some of the plots are accounted for in the theory. The magnitude of the coupling strength being 2 is relatively large because the PRCs have norm 1 and the phases vary from [0,1), and despite this, the fine details of the phase difference density are captured. There are a large number possible pairs to consider with $N = 1000$, but this small subset illustrates the vast range of synchronous behavior within the *same* network.

When the pulses decay slower ($\beta = 5$), the reduction theory still holds but the coupling strength α cannot be as large. In Figure 3.3, we consider $\alpha = -1$ and 1 to illustrate that the value of the theory. When the coupling strength $|\alpha| > 1$, there are significant differences compared to the Monte Carlo simulations (not shown) that will be apparent in subsequent figures (Figure 3.4). For inhibitory coupling, the theory

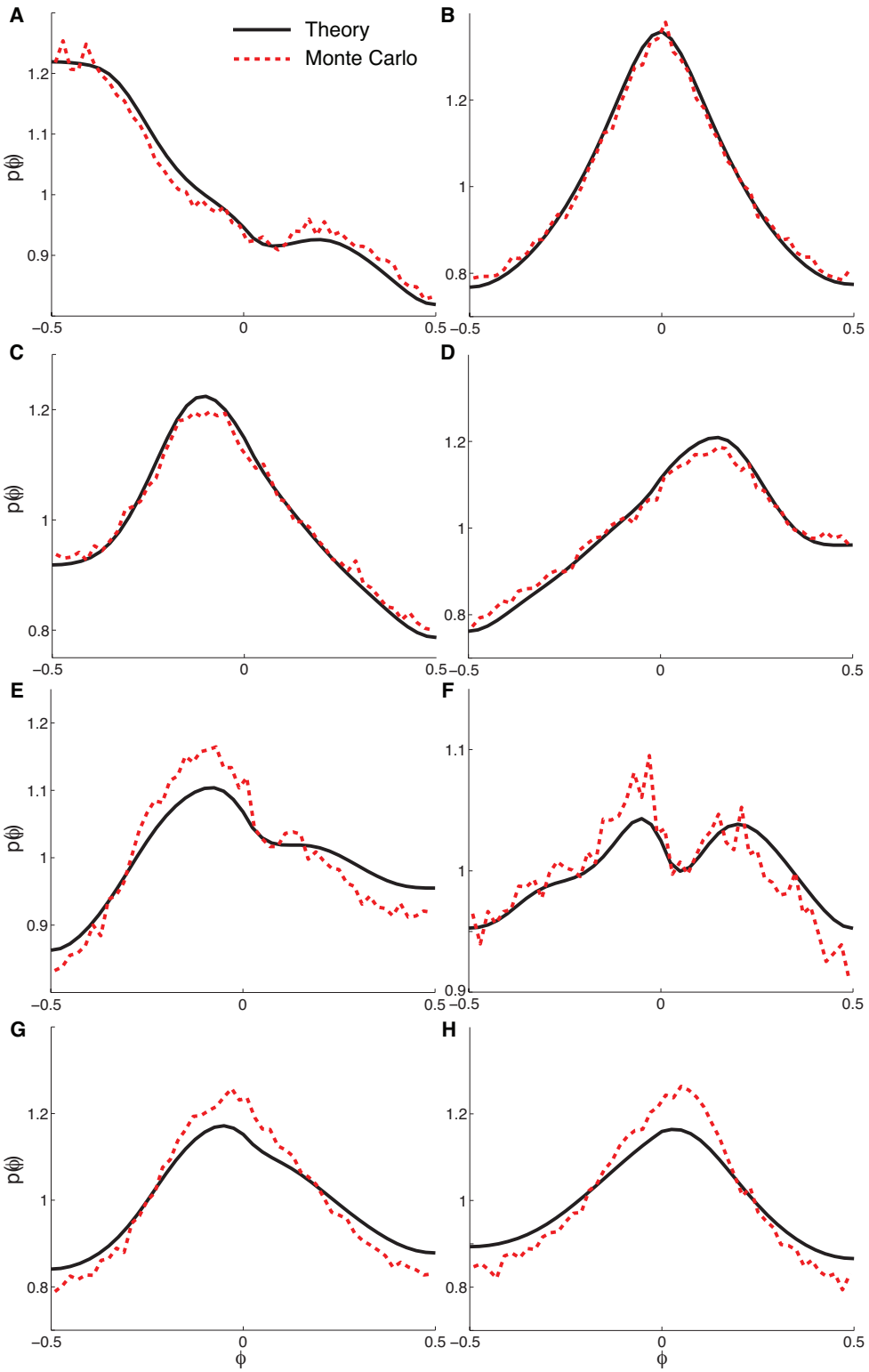

FIG. 3.2. *Density of phase difference varies dramatically.*

With fast decaying pulses, there are a large variety of phase differences within the same network that are captured by the reduction method. Monte-Carlo simulations (red-dashed; 500,000 points) that capture the average time at various phase differences are plotted with the reduction method (black), equation (3.4), for particular pairs in the network. (A)–(D) with inhibitory coupling $\alpha = -2$ and (E)–(H) with excitatory coupling $\alpha = 2$. The other parameters are: $\sigma = 0.3$, $c = 0.25$.

matches the Monte Carlo simulations well even with higher correlation and slower decaying pulses (Figure 3.3A–D). However, for large enough excitatory coupling $\alpha = 1$ (Figure 3.3E–F, there are deviations with the theory and the simulations. We only show two plots with excitatory coupling because almost all of the pairs considered had similar plots as shown; the system is in a regime of synchronous behavior (see Figure 3.4 and text surrounding this for more details). Notice the values of the vertical axes in Figure 3.3E–F; the pairs are pretty synchronous and the theory fails to capture the value of the peaks. In these cases, the net synchronous behavior is large because it is induced by coupling, correlated noise, *and* similar PRCs. Although this is alarming, the results are still good when $0 < |\alpha| \ll 1$ (not shown). In Figure 3.3 (in particular E, F), the correlation is higher than in Figure 3.2, and with slower decaying pulses the hypotheses of the theory are really being challenged because the noisy phases are likely more correlated and the conditional density cannot be well approximated by the unconditioned density. In this case, the total effect of coupling with slower decaying pulses is much larger on average, which goes against the weak coupling assumptions in the theory.

As coupling varies from inhibitory to excitatory ($\alpha \in [-2, 2]$), the same pair of neurons can exhibit rich behavior that is also captured by the method (not shown). Along these lines, we next study how the entire network dynamics change as coupling changes. With such numerous pairs, it is not feasible to consider the entire set of density of phase differences of all pairs. Another useful measure is the order parameter (O.P.) [28]:

$$\text{O.P.} = \int p(\phi) e^{-2\pi\phi}\, d\phi \in \mathbb{C} \tag{3.11}$$

which has the advantage of assigning a complex number to an entire phase difference density function $p(\phi)$. The O.P. has both a magnitude and an angle $O.P. = \|O.P.\|e^{i\varphi}$; the magnitude is a measure of how locked the pair is and the angle is an approximation of the phase lag (first Fourier mode) with values $\varphi \in [-\pi, \pi]$. For a given set of parameters, the entire range of pairwise dynamics is measured by the set of O.P. angles and O.P. magnitudes. Figure 3.4 shows the extreme values of the O.P. for all $N(N-1)/2$ pairs, where panels A–B is for the fast pulses and corresponding parameters in Figure 3.2 and panels C–D is for slower pulse parameters in Figure 3.3. The two red curves in each plot are the maximal and minimal values of the O.P.; all of the pairs in the network have O.P. values between these two curves. The previously described reduction method (black) is used to approximate the extremal values. Determining the actual pairs of neurons (PRCs) that correspond to the maximum and minimal O.P. angle and O.P. magnitude is a very interesting and complicated problem beyond the scope of this paper. The black curves were calculated by using the results of the Monte Carlo simulations; the specific pairs that corresponded to the maximum and minimum were used in the reduction method. This depends on coupling, among other parameters, and is different depending on whether the angle or magnitude of O.P. are considered.

The two regimes considered ($\beta = 50$ or 5) with the specific noise σ and input correlation c have different amounts of synchrony depending on coupling. Specifically, |O.P.| is larger on average, which is not surprising considering c is higher and the effect of a pulse is longer lasting. Here, a global picture of the reduction method shows that it is inaccurate for the magnitude of O.P. (Figure 3.4D). The range of O.P. angles change similarly as coupling increases, they both have a narrower range around 0 indicating that the best estimation of the peak(s) is around a 0 phase difference. Interestingly, the

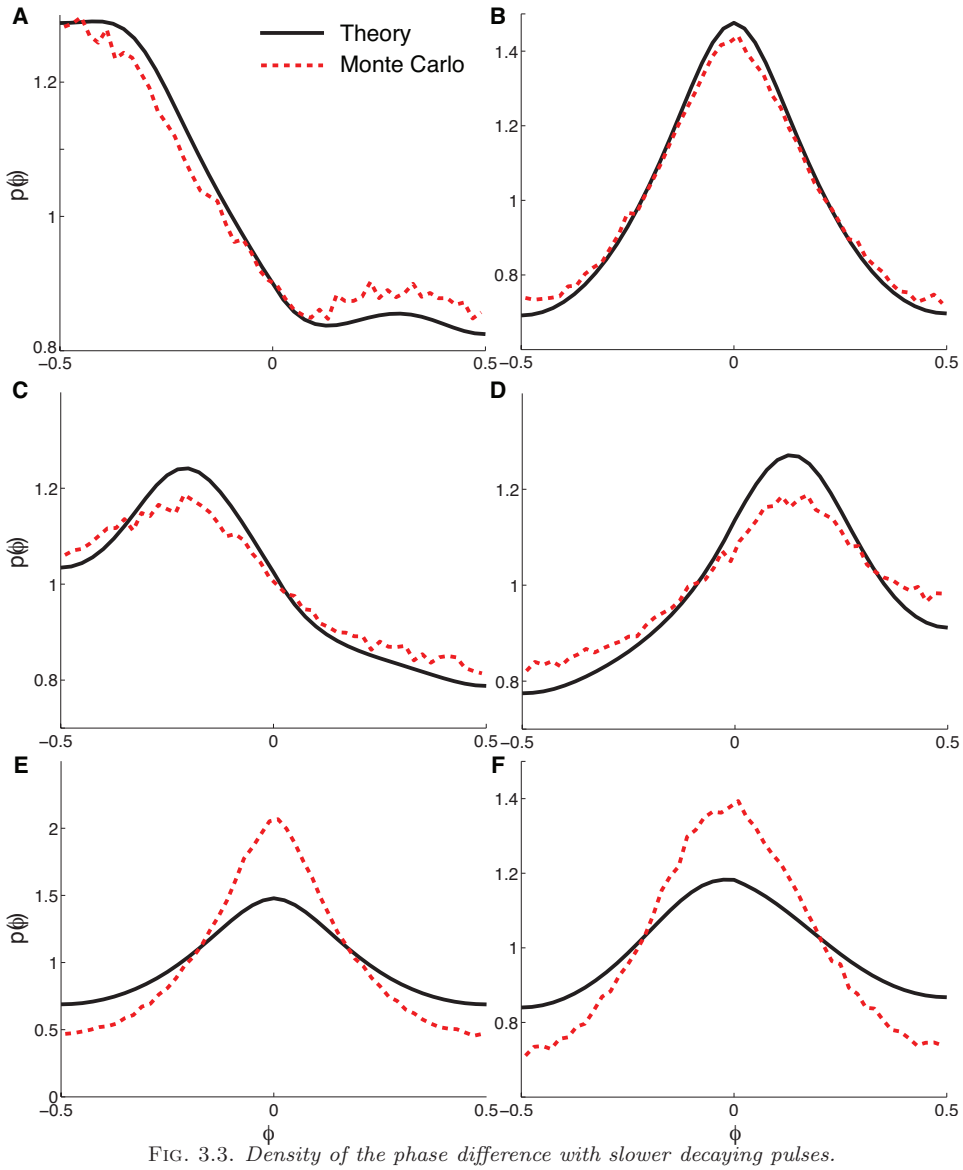

FIG. 3.3. *Density of the phase difference with slower decaying pulses.*
Similar format as Figure 3.2 but with $\beta = 5$. Monte-Carlo simulations (red-dashed; 500,000 points) that capture the average time at various phase differences are plotted with the reduction method (black), equation (3.4), for particular pairs in the network. (A)–(D) with inhibitory coupling $\alpha = -1$ and (E)–(F) with excitatory coupling $\alpha = 1$. The other parameters are $\sigma = 0.22$, $c = 0.35$.

|O.P.| range tends to increase with coupling. Although this type of coupling generally leads to more synchrony overall, the range of |O.P.| can increase while the range of possible O.P. angles decreases. It is strange that coupling can increase synchrony or phase-locking, but at the same time the range of |O.P.| increases. Further analysis reveals that pairs with vastly different Δ's have non-monotonic |O.P.| because they tend to be phase lagged with sharp peaks at $\phi \approx \pm 0.5$ when $\alpha < 0$, but as coupling

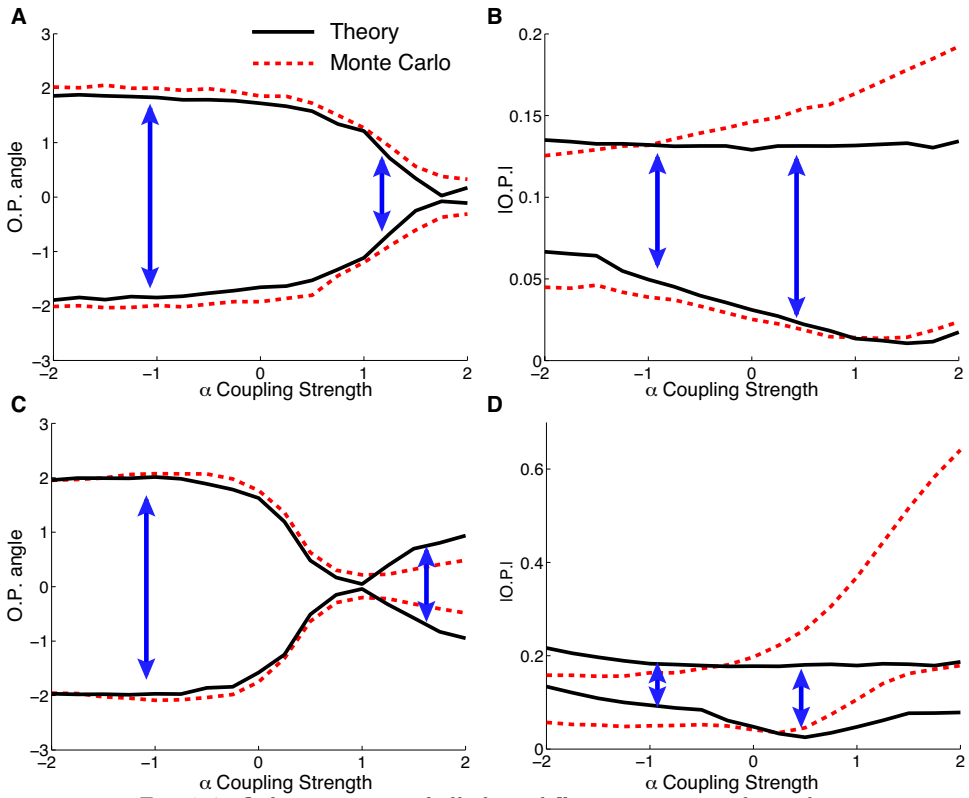

FIG. 3.4. *Order parameter of all phase differences varies with coupling.* (A)–(B) Fast pulses ($\beta = 50$) with $\sigma = 0.3$, $c = 0.25$: the O.P. angle and magnitude take on a range of values. The red dashed curves are the maximal and minimal values of these quantities from Monte Carlo simulations, and the black curves are similarly computed using the reduction method. For a given α, the pairs that correspond to the maximum and minimum values are complicated (see main text), and thus, the Monte Carlo simulation results are used to specify the pair of PRCs used in reduction method. (C)–(D) same as (A)–(B) but with slower pulses and $\sigma = 0.22$, $c = 0.35$. The blue arrows indicate a common trend that the range of O.P. angles decreases and range of O.P. magnitudes increase as α increases.

increases the pairs tend to be almost asynchronous (smaller |O.P.|) until finally they are locked at smaller phase differences (with larger |O.P.|). Also contributing to the increased range are the pairs that are sharply peaked at $\phi \approx 0$, who's |O.P.| values increase appreciably with coupling.

3.2. Comparison with a Morris-Lecar network model. This section makes a qualitative connection to a realistic neural oscillator network that satisfies some of the hypotheses of the previously described phase reduction and dimension reduction method in section 3. The network of Morris-Lecar oscillators [40] consists of 6 different types with different PRCs (see Appendix B for equations). We did not consider more distinct oscillators because ensuring they each had approximately the same intrinsic period and similar L_2-norms was extremely tedious. Another issue is that we want the effect of coupling and noisy inputs to be similar across the distinct types, which does not hold if the parameters vary greatly. To increase the size of

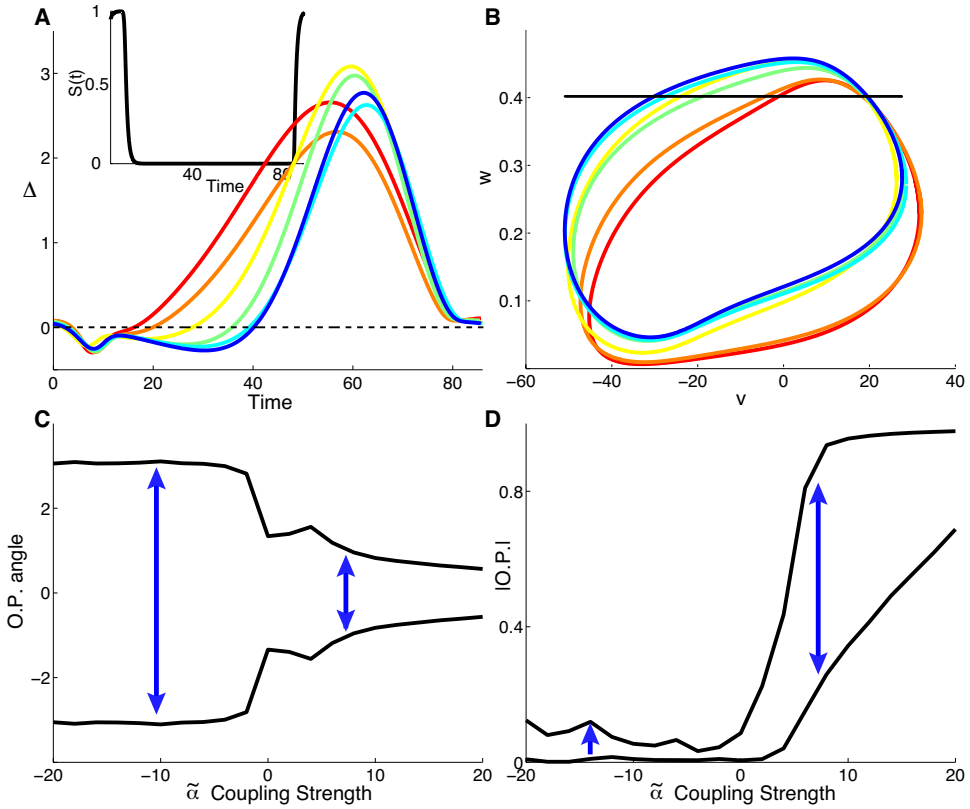

FIG. 3.5. *Morris-Lecar network.*

(A) The 6 distinct PRCs, with synapses (black, inset) for an all-to-all coupled network. (B) Unperturbed limit cycles, the thin black line is the threshold $w_{th} = 0.4$ for spiking as the w variable crosses from below. (C) Range of O.P. angles as coupling varies. (D) Range of |O.P.| as coupling varies. For (C)–(D), $\tilde{\sigma} = 0.01$ and $c = 0.3$ (see Appendix B for equations and parameter values).

network, there are 4 copies of each of the 6 distinct oscillator types, for a total network size of 24. The reason for doing is that a smaller network have different dynamics, and the random phases can be highly correlated with the other phases, especially with increased coupling strength. Figure 3.5 shows the distinct oscillators' PRCs (calculated via XPP [16]), synaptic dynamics in an unperturbed period (A, inset), and unperturbed limit cycles (B).

To resemble the phase oscillator network in a more direct way, the coupling is all-to-all and the synapses are current-based rather than conductance-based. With conductance-based synapses, the effects of coupling would depend on the chosen reversal potentials and have overall more complex dynamics. Figure 3.5C–D only shows the statistically distinct pairs of phase differences, with 6 different PRCs there are 15 unique pairs. The possible O.P. angles and |O.P.| as coupling $\tilde{\alpha}$ varies is complicated. Not surprisingly, the exact range of O.P. values in the Morris-Lecar network and the reduced phase oscillators do not exactly match because the phase oscillators are a simplification and the noise and coupling parameters were chosen arbitrarily. Nevertheless, there are some qualitative features that are shared between these networks. As coupling increases from inhibitory to excitatory, the range of O.P. angles decreases

and is centered around 0 (Figure 3.5C). Also, the range of values of |O.P.| tends to increase as coupling changes from inhibitory to excitatory, even though the network is more synchronous on average. These results were observed in the reduced phase oscillators (Figure 3.4). The coupling parameter $\tilde{\alpha}$ having absolute value up to 20 is not too large because the synapses are current-based, where $s_j(t) \in [0,1]$ is not multiplied by voltage. The coefficient of variation of time between spikes is around 0.1, indicating that the coupling and noise values are small enough to keep the neurons in the oscillator regime.

4. Variability of individual oscillators. In a stochastic neural network, the variability of the spike times of the distinct individual oscillators are important for a clearer picture of the dynamics of the network. Although the collective activity of the network is prominent in many systems, there are cases where a select sub-population plays a significant role. This section focusses on how pulse-coupling changes the variability of spiking, and in particular how variability depends on intrinsic heterogeneity (i.e., PRC type) in a coupled network.

Figure 4.1 shows the variance of the spike times as a function of coupling for the same phase oscillator networks described previously in section 2, with various values of β (duration of pulse), σ, and c. Interestingly, type I PRCs have larger $Var(T)$ with inhibitory pulse-coupling than type II PRCs, but with excitatory pulse-coupling type II PRCs have larger $Var(T)$ than Type I. This effect is robust to parameter changes so long as the overall coupling and noise are weak. Since this phenomena holds for $c = 0$ (Figure 4.1C and D), we focus on this case because it is still telling and the model is amenable to analysis.

Assuming $c = 0$ and the same assumptions as in section 3 where the effect of pulse-coupling is approximated by $\langle\langle P\rangle\rangle$, the individual neural obeys a simpler stochastic differential equation (equation (A.1)). The distribution of the time between spikes is governed by a modified Fokker-Planck equation [50], and the relevant statistics can be calculated with other methods (see [55] for some techniques). However, these methods are generally numerical and may not be as insightful as an asymptotic formula. Thus, the weak noise and weak coupling assumption are evoked to derive an analytic asymptotic formula for the $Var(T)$ in Appendix A. $Var(T)$ is approximated to fourth order by:

$$Var(T) \approx \sigma^2 + \sigma^4 E[T_3^2] + (\alpha\sigma)^2 E[T_5^2] + 2\alpha\sigma^2 E[T_1 T_5]. \tag{4.1}$$

The various terms are defined in equation (A.16) for an arbitrary Δ and P. The formulas are generally complicated, but when $\gamma = 0$ (Type II) and $\gamma = \pi/2$ (Type I), the formula provides an analytic explanation of the observed phenomena. The formula for these two canonical PRCs are:

$$E[T_3^2] = \begin{cases} \pi^2 & : \text{Type II} \\ \pi^2/3 & : \text{Type I} \end{cases} \tag{4.2}$$

$$E[T_5^2] = \begin{cases} 89/12 \\ \frac{16\pi^2}{27} + \frac{1295}{324} \end{cases} \approx \begin{cases} 7.42 & : \text{Type II} \\ 9.85 & : \text{Type I} \end{cases} \tag{4.3}$$

$$E[T_1 T_5] = \begin{cases} \frac{1}{2} - \frac{11\sqrt{2}}{12\pi} \\ \frac{1}{2} - \frac{11\sqrt{6}}{18} \end{cases} \approx \begin{cases} 0.087 & : \gamma = 0, \text{Type II} \\ -1 & : \gamma = \pi/2, \text{Type I} \end{cases} \tag{4.4}$$

These terms have varying effects on the variance: the top term $E[T_3^2]$ increases the variance independent of α with type II being 3 times larger than type I, although

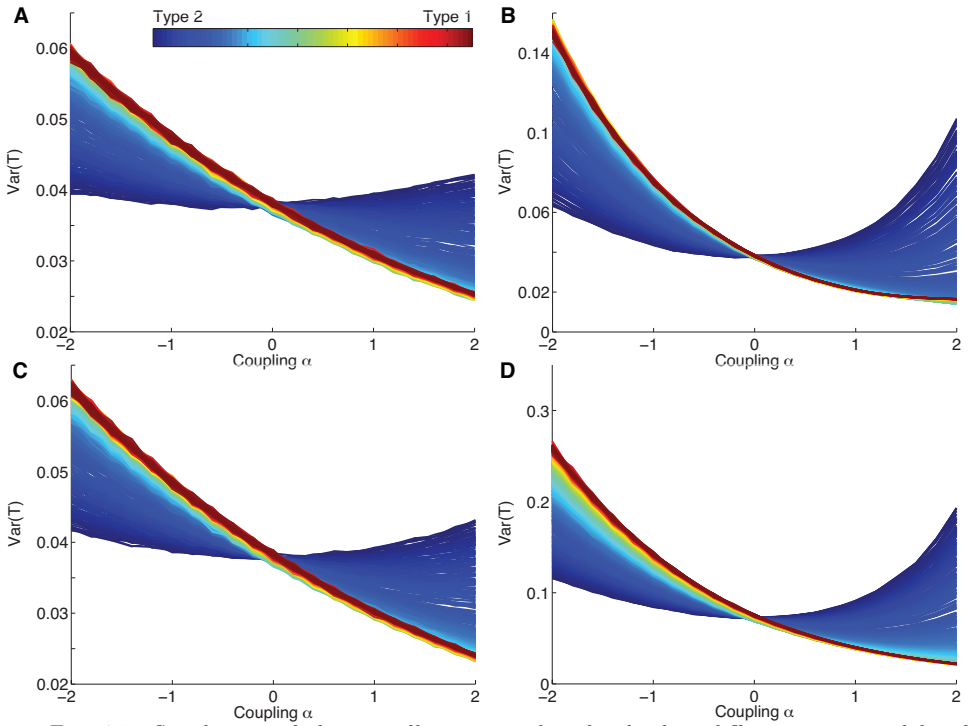

FIG. 4.1. *Simulations of phase oscillator networks robustly show differences in variability for Type I and Type II PRCs*
(A) $\beta = 50$, $\sigma = 0.2$, $c = 0.25$. (B) $\beta = 5$, $\sigma = 0.2$, $c = 0.35$. (C) $\beta = 50$, $\sigma = 0.2$, $c = 0$. (D) $\beta = 5$, $\sigma = 0.3$, $c = 0$. With all of these parameter sets, even when $c = 0$, type I has larger variability with inhibitory coupling but type II has larger variability with excitatory coupling.

this is a fourth order term. The middle fourth order term $E[T_5^2]$ increases $Var(T)$ equally for excitatory and inhibitory coupling (α^2) with type II being slightly smaller than type I. Finally, the signs ($+/-$) of the cross term $E[T_1T_5]$ explains the difference between excitatory ($\alpha > 0$) and inhibitory ($\alpha < 0$) coupling: for type II, inhibitory coupling decreases the variance while it increases it for type I. Analogously, excitatory coupling can increase the variance for type II but decreases it for type I. Note that this is the next order term beyond σ^2, which in general is $\sigma_2\|\Delta\|_2^2$ – recall that the L_2-norm of the PRC was set to 1.

4.1. Comparison to full oscillator models. The variance of the individual spikes in the same Morris-Lecar network considered in section 3.2 were analyzed to see if these quantities exhibited the same qualitative behavior as the reduced phase models in Figure 4.1. The results are in Figure 4.2A, and it obviously does not follow the same trend in the phase models (Figure 4.1). There seems to be a general decrease in the variance as coupling strength increases, but this does not hold for the orange curve which has a PRC with a large positive region (the red curve also shows a slight increase for some coupling values).

There could be several reasons for the discrepancy between the reduced phase models and Morris-Lecar model with regards to variability of spike times. There are many hypotheses that need to be satisfied, ranging from the phase reduction

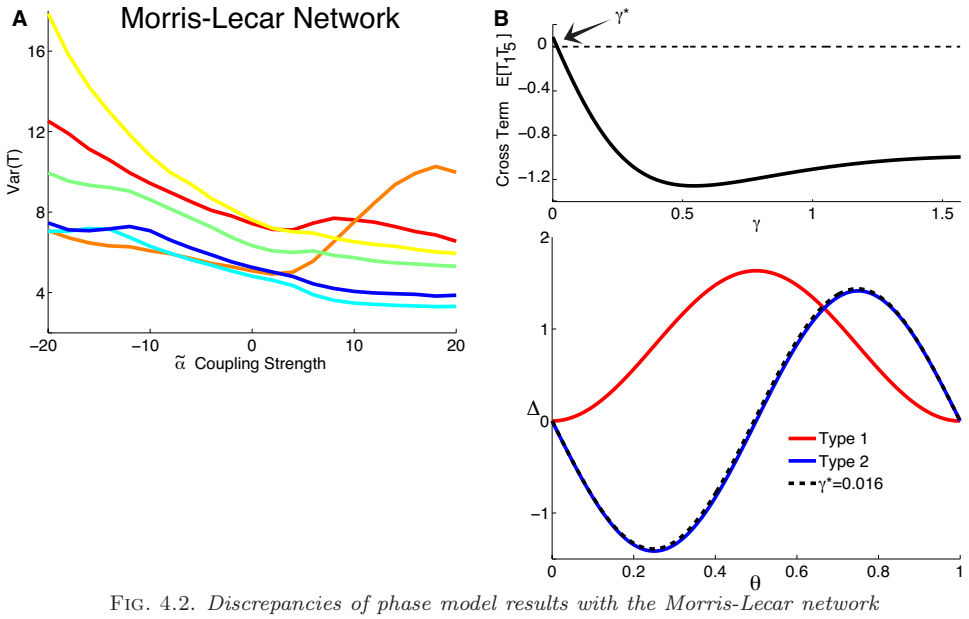

FIG. 4.2. *Discrepancies of phase model results with the Morris-Lecar network* (A) How the variability changes as a function of coupling is complicated in the Morris-Lecar network. Although there seems to be general trend of decreasing variability as coupling increases from inhibitory to excitatory, this is not always the case. Color-code and parameters are the same as in Figure 3.5. (B) Analysis of the phase oscillator network shows that the cross term $E[T_1T_5]$ as a function of a has to have almost sinusoidal PRC for the variance to increase with coupling, otherwise the variance decreases with coupling. The critical point γ^* where $E[T_1T_5] = 0$ is the threshold that whenever $\gamma \in (\gamma^*, \pi/2)$, the asymptotic theory suggests variability decreases with α.

hypotheses to the setup of the coupled network. A notable hypothesis is that the effect of coupling is approximated by average pulses that does not take into account correlation, and that the intrinsic dynamics (i.e., PRC) are the predominate factor for the differences in $Var(T)$. The asymptotic approximation of $Var(T)$ has many terms that each vary depending on the PRCs in the Morris-Lecar system, so that there is not an orderly categorization of the variance of T. We argue that observing the phenomena described in Figure 4.1 where the cross term $E[T_1T_5]$ is the main driver in differences for Type I and Type II, actually poses strict conditions on the PRC. The benefit of the analysis in equation (4.4) is that we can determine the critical value γ^* where $E[T_1T_5]$ vanishes, and it turns out that it is small $\gamma^* \approx 0.016$ (Figure 4.2B). Thus, the PRC has to be almost purely sinusoidal in order to observe an increase in the variability as coupling increases with type II like PRCs. The lower panel in Figure 4.2B shows the corresponding PRC to γ^* is almost indistinguishable with the purely sinusoidal PRC by visual inspection. This analysis shows in a clear way how only very specialized PRCs (in the phase oscillator network, not the Morris-Lecar system) leads to the observed phenomena of increased variability as α increases. Indeed, further inspection of Figure 4.1 shows that although many neurons have the described effect, they all have PRCs that are nearly sinusoidal (i.e., blue curves and uniform in color). Furthermore, there is a remarkable difference in the absolute values of the cross terms in equation (4.4); they defer by an order of magnitude suggesting non-robustness with

type II PRCs.

Other simulations of full oscillator models did not exhibit the orderly variability depending on PRC type that was observed in the phase oscillators. Many networks were considered, including a large population of just two distinct Morris-Lecar oscillators with type I and type II PRCs with the same frequencies, various noise levels $\tilde{\sigma}$ and background correlation c, and various synaptic dynamics (results not shown). A variety of type II PRCs were considered in these networks and still the effect was not observed; type II PRCs where there was bistability between oscillations and a stable rest state were naturally excluded because the high variability there is due to other reasons. Moreover, even in a Hodgkin Huxley neuron receiving noisy and artificial pulse inputs $\langle\langle P\rangle\rangle$, where the PRC has a relatively large negative region, the effect was not observed. We conclude that although reduced phase models have been successfully used in many situations to describe larger models and even real neurons, resulting analysis of phase oscillators can be misleading if not interpreted correctly. Specifically, we found purely sinusoidal PRCs to be misleading. We remark that the phase oscillator models are telling because they do show a lack of robustness of the phenomena upon closer examination.

5. Discussion. We studied a network of heterogeneous coupled noisy phase oscillators receiving correlated and independent noise. In any reasonable sized network ($N \geq 3$), characterizing the random behavior is intractable with probability density or Fokker-Planck equations. We have developed and presented a pragmatic reduction method to study the pairwise synchrony of distinct pairs of neural oscillators, assuming the conditional density of the phases is equal to the unconditional probability density. The method utilized our previous asymptotic results of noisy oscillators [34, 36]. The regimes where the method performed well and when it did not naturally depends on parameters. We have demonstrated the strengths and weaknesses in two different networks for exposition with explanations of how the underlying hypotheses might be violated. Specifically, when the pulse slowly decayed and when the background correlation was relatively large, the method only worked well with smaller coupling and noise values. We also studied the variability of the spike times in this network, and found a robust ordering of this statistic that depended on PRC type, where type I had larger variance with inhibitory pulse-coupling and type II had larger variance with excitatory pulse-coupling. These observations were explained with an insightful asymptotic formula.

The dynamics of coupled noisy phase oscillators are a deep an interesting area of study in their own right. Nevertheless, we attempted to make some connections to full oscillator models with varying levels of success. The qualitative behavior of the order parameters of distinct pairs as coupling varied generally matched a coupled Morris-Lecar system; namely, the range of the order parameter angles showed a stereotyped decrease centered around 0, and the range of the magnitude increases with coupling. The variability of the Morris-Lecar and other networks did not have the same behavior as observed in the phase oscillators. Asymptotic analysis revealed that the conditions on the PRC were stringent. Note that our analysis was only feasible with particular hypotheses that may not be satisfied in a full larger dimensional oscillator model. Recently, several authors have re-examined the phase reduction to a scalar model and have proposed alternatives with more variables and equations when the stimuli are not weak [56, 10, 29]. The work here does not address the case of strong stimuli, but a proper description of the analogous neural network with moderate to strong stimuli would be even more complicated and higher dimensional. However, such approaches

might be better at capturing the dynamics of the full oscillator models.

There are limitations to the work presented here and potential future directions. One avenue is to derive a better approximation for the 2-d Fokker-Planck equation for the density of the phase differences by taking into account dependence of the phases. There are certainly finite size effects that are not captured by a Fokker-Planck description [14, 8, 22] that remain to be addressed, especially in the Morris-Lecar network we have considered. The analysis of the variance of spike times, like the reduction method, assumes the effect of pulse coupling is well-approximated by averaging, and in particular the intrinsic PRCs is the main explanation of the phase oscillator results. Although not specifically addressed here, network effects can be just as important, especially when the all-to-all coupling assumption is relaxed. We have focused on pairwise synchrony, an instantaneous measure of co-varability. Other authors have considered correlation of oscillators for different window sizes of observation [6, 3, 5], a potential avenue of future work with correlated noise, coupling and heterogeneity.

Another realistic attribute that we did not consider is heterogeneous intrinsic frequencies. This would certainly lead to augmentations of the theory developed here. Simulations of networks with all of the previously described features and heterogeneous intrinsic frequencies show that the pairwise synchrony measured by order parameter (O.P.) changes in complicated ways (not shown). For the parameters we considered, the magnitude of O.P. does not vary much with frequency distributions compared to when all frequencies are identical. The O.P. angle has a wider range when there is more disorder in the intrinsic frequencies, as one might expect. For some distributions of frequency, the range of possible O.P. angle decreases with coupling as when the frequencies are identical. However, for other distributions of frequencies (more disorder), the range of possible angles can actually *increase* with coupling. Thus, these preliminary results may merit further investigation. The results for the reduced phase models for the variance of the period hold in a similar way with heterogeneous intrinsic frequencies. Simulations show that only a small subset of nearly type II PRCs show non-monotonic behavior as coupling strength increases (not shown). Similar analyses for this class of networks might be feasible, for example by allowing the intrinsic frequency 1 to be randomly drawn from a distribution yet be quenched. The effect of the pulse coupling would then have to account for random intrinsic frequencies as well. Since this randomness is quenched, one could average over this distribution after the calculations to access the utility of such an approach.

The interplay of heterogeneity in neural networks has been addressed by several authors [52, 11, 46, 9, 61, 59, 32]. Work most closely related to ours is Zhou et al. [61], who analyzed two heterogeneous uncoupled oscillators subject to correlated noise drive. They were able to derive asymptotic formulas for the steady-state probability density of the phase difference. Primarily based on simulations, Yim et al. [59] has considered uncoupled heterogeneous networks receiving external noisy inputs, and found heterogeneity can lead to de-correlation. In the context of neural coding, various authors have proposed that heterogeneity can decrease synchrony/correlation and generally increase information capacity [11, 46, 52] (however, see [1]). Thus, a deeper mechanistic understanding of heterogeneity in coupled stochastic neural networks in important and could impact other areas of computational neuroscience.

There is a large body of work concerning noisy oscillators in many areas. Many have studied them with coupling and uncorrelated noise in different contexts ([23, 20, 25, 26], to name a few). Noisy oscillators without coupling and correlated noise have been analyzed by [53, 42, 38], where correlated noise could lead to synchrony. Coupling

with correlated noise can lead to a range of synchronous or asynchronous behaviors [33, 62]. Here, we have considered a network with three combined attributes: intrinsic heterogeneity via PRC, correlated noise, and coupling. Lai & Porter [31] similarly had these three attributes in a Kuramoto type model with diffusive coupling where heterogeneity was in the intrinsic frequencies. They showed how coupling or noise (see [41] for a similar finding) could synchronize this network under suitable conditions. The study of noisy oscillator networks is a rich area with diverse applications ranging from neuroscience, ecology, etc.

Appendix A. Asymptotic expansion of the random spike time.

The following calculations are similar to the calculations in the appendix of [35], except that the theory has been applied to a heterogenous pulse-coupled network. With the same assumptions as in section 3, we approximate the effect of pulse-coupling $\langle\langle P\rangle\rangle$. We also assume no background correlation $c = 0$ to streamline the analysis (see Section 4), so that an individual oscillator starting from $\Theta_j(0) = 0$ has the following equation:

$$\Theta_j(t) = t + \frac{\sigma^2}{2}\int_0^t \Delta_j(\Theta_j(s))\Delta_j'(\Theta_j(s))\,ds + \alpha\,\langle\langle P\rangle\rangle \int_0^t \Delta_j(\Theta_j(s))\,ds + \sigma\int_0^t \Delta_j(\Theta_j(s))\,dW(s) \tag{A.1}$$

where $dW(s)$ denotes integrating against white noise (i.e., stochastic integral). Assume $\sigma = O(\varepsilon)$ and $\alpha = O(\varepsilon)$, and expand the last 3 terms above to get:

$$\frac{\sigma^2}{2}\int_0^t \Delta_j(\Theta_j(s))\Delta_j'(\Theta_j(s))\,ds = \frac{\sigma^2}{2}\frac{\Delta_j^2(t)}{2} + O(\varepsilon^3) \tag{A.2}$$

$$\begin{aligned}\alpha\,\langle\langle P\rangle\rangle \int_0^t \Delta_j(\Theta_j(s))\,ds = {}& \alpha\,\langle\langle P\rangle\rangle \int_0^t \Delta_j(s)\,ds \\ & + \alpha\sigma\,\langle\langle P\rangle\rangle \int_0^t \Delta_j'(s)\int_0^s \Delta_j(r)\,dW(r)\,ds \\ & + \alpha^2\,\langle\langle P\rangle\rangle^2 \int_0^t \Delta_j'(s)\int_0^s \Delta_j(r)\,dr\,ds + O(\varepsilon^3)\end{aligned} \tag{A.3}$$

$$\begin{aligned}\sigma\int_0^t \Delta_j(\Theta_j(s))\,dW(s) = {}& \sigma\int_0^t \Delta_j(s)\,dW(s) \\ & + \sigma^2\int_0^t \Delta_j'(s)\int_0^s \Delta_j(r)\,dW(r)\,dW(s) \\ & + \alpha\sigma\,\langle\langle P\rangle\rangle \int_0^t \Delta_j'(s)\int_0^s \Delta_j(r)\,dr\,dW(s) + O(\varepsilon^3)\end{aligned} \tag{A.4}$$

Using this expansion, we collect the terms with the same coupling and/or noise coefficients in equation (A.1):

$$\Theta_j(t) = t + \sigma Z_1(t) + \alpha Z_2(t) + \sigma^2 Z_3(t) + \alpha^2 Z_4(t) + \alpha\sigma Z_5(t) + O(\varepsilon^3) \tag{A.5}$$

where the random variables $Z_j(t)$ are:

$$Z_1(t) = \int_0^t \Delta_j(s)\,dW(s) \tag{A.6}$$

$$Z_2(t) = \langle\langle P\rangle\rangle\,\tilde{\Delta}_j(t) \tag{A.7}$$

$$Z_3(t) = \frac{1}{4}\Delta_j^2 + \int_0^t \Delta_j'(s) \int_0^s \Delta_j(r)\, dW(r)\, dW(s) \tag{A.8}$$

$$Z_4(t) = \langle\langle P \rangle\rangle^2 \int_0^t \Delta_j'(s) \int_0^s \Delta_j(r)\, dr\, ds \tag{A.9}$$

$$\begin{aligned} Z_5(t) &= \langle\langle P \rangle\rangle \int_0^t \Delta_j'(s) \int_0^s \Delta_j(r)\, dW(r)\, ds \\ &\quad + \langle\langle P \rangle\rangle \int_0^t \Delta_j'(s) \int_0^s \Delta_j(r)\, dr\, dW(s); \end{aligned} \tag{A.10}$$

Here, we have denoted the integral of the PRC by $\tilde{\Delta}_j$:

$$\tilde{\Delta}_j(t) := \int_0^t \Delta_j(s)\, ds.$$

We want the statistics of the random period T, where $\Theta_j(T) = 1$. We thus asymptotically expand around T:

$$T = 1 + \sigma T_1 + \alpha T_2 + \sigma^2 T_3 + \alpha^2 T_4 + \alpha\sigma T_5 + O(\varepsilon^3); \tag{A.11}$$

substitute this formula into $\Theta_j(T) = 1$ and use equation (A.5) to get:

$$1 = \Big(1+\sigma T_1+\alpha T_2+\sigma^2 T_3+\alpha^2 T_4+\alpha\sigma T_5\Big)+\sigma Z_1(T)+\alpha Z_2(T)+\sigma^2 Z_3(T)+\alpha^2 Z_4(T)+\alpha\sigma Z_5(T) \tag{A.12}$$

Solving for the T_k's entails expanding the Z_k's around 1, collecting terms with the same coefficients while ignoring the $O(\varepsilon^3)$ terms, and solving the equation term by term (set each term to 0 since the 1's cancel). Each of the five coefficients in α/σ give the following five equations:

$$\begin{aligned} T_1 &= -Z_1(1) \\ T_2 &= -Z_2(1) \\ T_3 &= -Z_3(1) - Z_1'(1)T_1 \\ T_4 &= -Z_4(1) - Z_2'(1)T_2 \\ T_5 &= -Z_5(1) - Z_1'(1)T_2 - Z_2'(1)T_1 \end{aligned}$$

The mean of T, $\mu(T)$, to second order is obtained by averaging equation (A.11)

$$\mu(T) = 1 - \alpha \langle\langle P \rangle\rangle \int_0^1 \Delta_j(s)\, ds - (\alpha \langle\langle P \rangle\rangle)^2 \int_0^1 \Delta_j^2(s)\, ds + O(\varepsilon^3) \tag{A.13}$$

and the variance of T is

$$\begin{aligned} Var(T) &= E\Big[(T - \mu(T))^2\Big] \\ &= E\Big[\, \big(\sigma T_1 + \sigma^2 T_3 + \alpha\sigma T_5\big)^2 \,\Big] + O(\varepsilon^5) \\ &= \sigma^2 E[T_1^2] + \sigma^4 E[T_3^2] + (\alpha\sigma)^2 E[T_5^2] + 2\alpha\sigma^2 E[T_1 T_5] + O(\varepsilon^5) \end{aligned} \tag{A.14}$$

The terms $2\sigma^3 E[T_1 T_3]$ and $2\alpha\sigma^3 E[T_3 T_5]$ vanish because odd powers of noise in the stochastic integrals vanish: $E[dW^{2n-1}] = 0$. The only left to calculate are the expected values in equation (A.14). By Itô isometry,

$$E[T_1^2] = E\left[\left(\int_0^1 \Delta_j(s)\, dW(s)\right)^2\right] = \int_0^1 (\Delta_j(s))^2\, ds = 1 \tag{A.15}$$

Recall that L_2-norm of the PRC is set to 1. The subsequent terms of interest are all calculated with properties of white noise (i.e., $E[dW(s)dW(r)] = \delta(r-s)\,drds$), Fubini's theorem, and integration by parts. The results are:

$$\begin{aligned}
E[T_3^2] &= \frac{1}{2}\int_0^1 (\Delta_j'(s))^2 \int_0^s (\Delta_j(r))^2\,dr\,ds \\
E[T_5^2] &= \langle\langle P\rangle\rangle^2 \Big[\int_0^1 [\Delta_j'(s)\tilde{\Delta}_j(s)]^2\,ds - 2\int_0^1 \Delta_j(s)^2\Delta_j'(s)\tilde{\Delta}_j(s)\,ds \\
&\quad +2\int_0^1 (1-s)\left[\Delta_j'(s)\right]^2\Delta_j(s)\tilde{\Delta}_j(s)\,ds + \int_0^1 \Delta_j^4(s)\,ds\Big] \\
E[T_1T_5] &= \langle\langle P\rangle\rangle \Big[\int_0^1 (1-s)\left[\Delta_j'(s)\Delta_j(s)\tilde{\Delta}_j(s) + \Delta_j^2(s)\right]\,ds \\
&\quad + \int_0^1 \Delta_j(s)\int_0^s \Delta_j'(r)\tilde{\Delta}_j(r)\,dr\,ds - \int_0^1 \Delta_j^3(s)\,ds\Big]
\end{aligned} \tag{A.16}$$

Equations (A.14)–(A.16) are used to describe how the variance of spike time changes with coupling.

Appendix B. Morris-Lecar Equations.

The network of N Morris-Lecar oscillators [40] with shared and unshared noise and all-to-all synaptic (current-based) coupling have the follow equations:

$$\begin{aligned}
C\frac{dv_j}{dt} &= I_{app,j} - g_l(v_j-\varepsilon_l) - g_k w_j(v_j)(v_j-\varepsilon_k) - g_{ca}m_\infty(v_j)(v_j-\varepsilon_{ca}) \\
&\quad +\tilde{\alpha}\sum_{k\neq j} s_k(v_k) + \tilde{\sigma}\xi_j(t)
\end{aligned} \tag{B.1}$$

$$\frac{dw_j}{dt} = \varphi_j\frac{w_\infty(v_j)-w_j(v_j)}{\tau_w(v_j)} \tag{B.2}$$

$$\frac{ds_j}{dt} = s_\infty(v_j) - s_j \tag{B.3}$$

with $\langle\xi_j(t)\rangle = 0$, and $\langle\xi_j(t)\xi_i(t')\rangle = \delta_{ij}c\delta(t-t')$. The auxiliary functions are:

$$\begin{aligned}
m_\infty(v) &= 0.5\cdot(1+\tanh((v-v_a)/v_b)) \\
w_\infty(v) &= 0.5\cdot(1+\tanh((v-v_c)/v_d)) \\
\tau_w(v) &= \frac{1}{\cosh((v-v_c)/(2v_d))} \\
s_\infty(v) &= 0.5\cdot(1+\tanh((v-v_{s1})/v_{s2}))
\end{aligned}$$

The parameter values in Figure 3.5 are: $C = 20\frac{\mu F}{cm^2}$, $g_l = 2\,\frac{mS}{cm^2}$, $\varepsilon_l = -60\,\mathrm{mV}$, $g_k = 8\,\frac{mS}{cm^2}$, $\varepsilon_k = -84\,\mathrm{mV}$, $g_{ca} = 4\,\frac{mS}{cm^2}$, $\varepsilon_{ca} = 120\,\mathrm{mV}$. For the auxiliary functions: $v_a = -1.2\,\mathrm{mV}$, $v_b = 18\,\mathrm{mV}$, $v_{s1} = 20\,\mathrm{mV}$, $v_{s2} = 1\,\mathrm{mV}$.

The variables I_{app}, φ, v_c, v_d were different for each of the six types of oscillators, and had the following values (Figure 3.5: **i** is red, **vi** is blue):

Appendix C. Acknowledgments. We thank Bard Ermentrout for useful conversations.

REFERENCES

ML Type	i	ii	iii	iv	v	vi
I_{app} ($\mu A/cm^2$)	47	49.5	57	65.5	66	68
φ (ms^{-1})	2/30	0.06	0.06	0.06	0.05	0.05
v_c (mV)	12	11	5	8	5	4
v_d (mV)	17	18	20	25	23	23

[1] L.F. Abbott and P. Dayan, *The effect of correlated variability on the accuracy of a population code*, Neural Computation, 11 (1999), pp. 91–101.

[2] A. Abouzeid and B. Ermentrout, *Type-ii phase resetting curve is optimal for stochastic synchrony*, Physical Review E, 80 (2009), p. 011911.

[3] ———, *Correlation transfer in stochastically driven neural oscillators over long and short time scales*, Physical Review E, 84 (2011), p. 061914.

[4] J.A. Acebrón, L.L Bonilla, C.J.P. Vicente, F. Ritort, and R. Spigler, *The kuramoto model: A simple paradigm for synchronization phenomena*, Reviews of modern physics, 77 (2005), p. 137.

[5] A.K. Barreiro, E.L. Thilo, and E. Shea-Brown, *A-current and type i/type ii transition determine collective spiking from common input*, Journal of Neurophysiology, 108 (2012), p. 1631.

[6] A. K. Barreiro, E. Shea-Brown, and E.L. Thilo, *Time scales of spike-train correlation for neural oscillators with common drive*, Physical Review E, 81 (2010), p. 011916.

[7] P.C. Bressloff and Y.M. Lai, *Stochastic synchronization of neuronal populations with intrinsic and extrinsic noise*, The Journal of Mathematical Neuroscience, 1 (2011), pp. 1–28.

[8] M.A. Buice and C.C. Chow, *Correlations, fluctuations, and stability of a finite-size network of coupled oscillators*, Physical Review E, 76 (2007), p. 031118.

[9] S.D. Burton and B. Ermentrout N.N. Urban, *Intrinsic heterogeneity in oscillatory dynamics limits correlation-induced neural synchronization*, Journal of Neurophysiology, 108 (2012), pp. 2115–2133.

[10] O. Castejón, A. Guillamon, and G. Huguet, *Phase-amplitude response functions for transient-state stimuli*, The Journal of Mathematical Neuroscience, 3 (2013), pp. 1–26.

[11] M.I. Chelaru and V. Dragoi, *Efficient coding in heterogeneous neuronal populations*, Proceedings of the National Academy of Sciences, 105 (2008), pp. 16344–16349.

[12] M.R. Cohen and A. Kohn, *Measuring and interpreting neuronal correlations*, Nature Neuroscience, 14 (2011), pp. 811–819.

[13] S. Coombes and P.C. Bressloff, *Mode locking and Arnold tongues in integrate-and-fire neural oscillators*, Physical Review E, 60 (1999), pp. 2086–2096.

[14] H. Daido, *Intrinsic fluctuations and a phase transition in a class of large populations of interacting oscillators*, Jouranl of Statistical Physics, 60 (1990), pp. 753–800.

[15] B. Ermentrout, *Type I membranes, phase-resetting curves, and synchrony*, Neural Computation, 8 (1996), pp. 979–1001.

[16] ———, *Simulating, Analyzing, and Animating Dynamical Systems: A Guide to XPPAUT for Researchers and Students*, SIAM, 2002.

[17] B. Ermentrout, M. Pascal, and B. Gutkin, *The effects of spike frequency adaptation and negative feedback on the synchronization of neural oscillators*, Neural Computation, 13 (2001), pp. 1285–1310.

[18] R.F. Galán, N. Fourcaud-Trocmé, B. Ermentrout, and N.N. Urban, *Correlation-induced synchronization of oscillations in olfactory bulb neurons*, The Journal of Neuroscience, 26 (2006), pp. 3646–3655.

[19] C.W. Gardiner, *Handbook of stochastic methods*, Springer-Verlag, 1985.

[20] D. Hansel and G. Mato, *Asynchronous States and the Emergence of Synchrony in Large Networks of Interacting Excitatory and Inhibitory Neurons*, Neural Computation, 15 (2003), pp. 1–56.

[21] D. Hansel, G. Mato, and C. Meunier, *Synchrony in excitatory neural networks*, Neural Computation, 7 (1995), pp. 307–337.

[22] E.J. Hildebrand, M.A. Buice, and C.C. Chow, *Kinetic theory of coupled oscillators*, Physical Review Letters, 98 (2007), p. 054101.

[23] E.M. Izhikevich, *Phase equations for relaxation oscillators*, SIAM Journal on Applied Mathematics, 60 (2000), pp. 1789–1804.

[24] E. M. Izhikevich, *Weakly pulse-coupled oscillators, FM interactions, synchronization, and oscillatory associative memory*, IEEE Transactions on Neural Networks, 10 (1999), pp. 508–

526.
[25] T. Kanamaru, *Analysis of Synchronization Between Two Modules of Pulse Neural Networks with Excitatory and Inhibitory Connections*, Neural Comput., 18 (2006), pp. 1111–1131.
[26] T. Kanamaru and K. Aihara, *Stochastic synchrony of chaos in a pulse-coupled neural network with both chemical and electrical synapses among inhibitory neurons*, Neural Comput., 20 (2008), pp. 1951–1972.
[27] B. W. Knight, *Dynamics of Encoding in a Population of Neurons*, Journal of General Physiology, 59 (1972), pp. 734–766.
[28] Y. Kuramoto, *Chemical Oscillations, Waves and Turbulence.*, Springer-Verlag, New York, 1984.
[29] W. Kurebayashi, S. Shirasaka, and H. Nakao, *Phase reduction method for strongly perturbed limit cycle oscillators*, Physical Review Letters, 111 (2013), p. 214101.
[30] Y.M. Lai, J. Newby, and P.C. Bressloff, *Effects of demographic noise on the synchronization of a metapopulation in a fluctuating environment*, Physical review letters, 107 (2011), p. 118102.
[31] Y.M. Lai and M.A. Porter, *Noise-induced synchronization, desynchronization, and clustering in globally coupled nonidentical oscillators*, Physical Review E, 88 (2013), p. 012905.
[32] T.B. Luke, E. Barreto, and P. So, *Complete classification of the macroscopic behavior of a heterogeneous network of theta neurons*, Neural Computation, 25 (2013), pp. 3207–3234.
[33] C. Ly and B. Ermentrout, *Synchronization dynamics of two coupled neural oscillators receiving shared and unshared noisy stimuli*, Journal of Computational Neuroscience, 26 (2009), pp. 425–443.
[34] ———, *Analysis of recurrent networks of pulse-coupled noisy neural oscillators*, SIAM Journal on Applied Dynamical Systems, 9 (2010), pp. 113–137.
[35] ———, *Coupling regularizes individual units in noisy populations*, Physical Review E, 81 (2010), p. 011911.
[36] C. Ly and B. Ermentrout, *Analytic approximations of statistical quantities and response of noisy oscillators*, Physica D, 240 (2011), pp. 719–731.
[37] E. Marder, *Variability, compensation, and modulation in neurons and circuits*, Proceedings of the National Academy of Sciences, 108 (2011), pp. 15542–15548.
[38] S. Marella and B. Ermentrout, *Class-ii neurons display a higher degree of stochastic synchronization than class-i neurons*, Physical Review E, 77 (2008), p. 041918.
[39] R. E. Mirollo and S.H. Strogatz, *Synchronization of pulse-coupled biological oscillators*, SIAM Journal of Applied Mathematics, 50 (1990), pp. 1645–1662.
[40] C. Morris and H. Lecar, *Voltage oscillations in the barnacle giant muscle fiber*, Biophysical Journal, 35 (1981), pp. 193–213.
[41] K.H. Nagai and H. Kori, *Noise-induced synchronization of a large population of globally coupled nonidentical oscillators*, Physical Review E, 81 (2010), p. 065202.
[42] H. Nakao, K. Arai, and Y. Kawamura, *Noise-induced synchronization and clustering in ensembles of uncoupled limit-cycle oscillators*, Phys. Rev. Lett., 98 (2007), p. 184101.
[43] J. M. Newby and M. A. Schwemmer, *Effects of moderate noise on a limit cycle oscillator: Counter rotation and bistability*, Physical Review Letters, (2014), p. (in press).
[44] S. Ostojic, N. Brunel, and V. Hakim, *How connectivity, background activity, and synaptic properties shape the cross-correlation between spike trains*, The Journal of Neuroscience, 29 (2009), pp. 10234–10253.
[45] S. Ostojic, N. Brunel, and V. Hakim, *Synchronization properties of networks of electrically coupled neurons in the presence of noise and heterogeneities*, Journal of Computational Neuroscience, 26 (2009), pp. 369–392.
[46] K. Padmanabhan and N.N. Urban, *Intrinsic biophysical diversity decorrelates neuronal firing while increasing information content*, Nature Neuroscience, 13 (2010), pp. 1276–1282.
[47] B. Pfeuty, G. Mato, D. Golomb, and D. Hansel, *The Combined Effects of Inhibitory and Electrical Synapses in Synchrony*, Neural Computation, 17 (2005), pp. 633–670.
[48] A.A. Prinz, N.W. Schultheiss, and R.J. Butera, *Phase Response Curves in Neuroscience*, Springer, 2012.
[49] J. Rinzel and B. Ermentrout, *Analysis of neural excitability and oscillations*, in Methods in Neuronal Modeling: From Synapses to Networks, I. Segev, ed., MIT Press, 1989, pp. 135–169.
[50] H. Risken, *The Fokker-Planck equation: methods of solutions and applications*, Springer-Verlag, New York, NY, 1989, ch. 1.
[51] R. Rosenbaum, J. Trousdale, and K. Josić, *Pooling and correlated neural activity*, Frontiers in Computational Neuroscience, 4 (2010).
[52] M. Shamir and H. Sompolinsky, *Implications of neuronal diversity on population coding*,

Neural Computation, 18 (2006), pp. 1951–1986.
[53] J. Teramae and D. Tanaka, *Robustness of the noise-induced phase synchronization in a general class of limit cycle oscillators*, Physical Review Letters, 93 (2004), p. 204103.
[54] J. N. Teramae, H. Nakao, and B. Ermentrout, *Stochastic phase reduction for a general class of noisy limit cycle oscillators*, Physical Review Letters, 102 (2009), p. 194102.
[55] J. Touboul and O. Faugeras, *The spikes trains probability distributions: a stochastic calculus approach*, Journal of Physiology-Paris, 101 (2007), pp. 78–98.
[56] K. CA Wedgwood, K. Lin, R. Thul, and S. Coombes, *Phase-amplitude descriptions of neural oscillator models*, Journal of Mathematical Neuroscience, 3 (2013), p. 2.
[57] A. T. Winfree, *Patterns of phase compromise in biological cycles*, Journal of Mathematical Biology, 1 (1974), pp. 73–93.
[58] ———, *The geometry of biological time*, vol. 12, Springer, 2001.
[59] M.Y. Yim, A. Aertsen, and S. Rotter, *Impact of intrinsic biophysical diversity on the activity of spiking neurons*, Physical Review E, 87 (2013), p. 032710.
[60] K. Yoshimura and K. Arai, *Phase reduction of stochastic limit cycle oscillators*, Physical Review Letters, 101 (2008), p. 154101.
[61] P. Zhou, S.D. Burton, N.N. Urban, and B. Ermentrout, *Impact of neuronal heterogeneity on correlated colored noise-induced synchronization*, Frontiers in Computational Neuroscience, 7 (2013).
[62] E.A. Zilli and M.E. Hasselmo, *Coupled noisy spiking neurons as velocity-controlled oscillators in a model of grid cell spatial firing*, The Journal of Neuroscience, 30 (2010), pp. 13850–13860.